2022

Frequency Analysis of Trabecular Bone Structure

Daniel Parada San Martin
University of Denver

Frequency Analysis of Trabecular Bone Structure

Abstract

Medical data is hard to obtain due to privacy laws making research difficult. Many databases of medical data have been compiled over the years and are available to the scientific community. These databases are not comprehensive and lack many clinical conditions. Certain type of medical conditions are rare, making them harder to obtain, or are not present at all in the aforementioned databases. Due to the sparsity or complete lack of data regarding certain conditions, research has stifled. Recent developments in machine learning and generative neural networks have made it possible to generate realistic data that can overcome the lack of data in the medical field. For example, the study of osteoporosis, poor bone density, or osteoarthritis, over abundance of bone material, has been studied extensively. Despite the commonality of these conditions, getting data is still difficult. This data is required to develop treatments but it is a problem that continues to plague an ever aging population. The ability to generate bone data with specific micro-structural parameters, enabling the simulation of real world data, for a desired medical condition would remove the high barrier that currently exists in the field.

This thesis explores fundamental properties of bone microstructure that can help describe said structure. This would provide insight into the bone spongiosa, the interior portion of bones, which contributes to bone stability. It explores the bone microstructure in the frequency space through the Fourier transform in order to explore useful properties, like isomorphism.

Document Type

Thesis

Degree Name

M.S.

Department

Computer Science

First Advisor

Haluk Ogmen

Second Advisor

Mario Lopez

Third Advisor

Catherine Durso

Keywords

Fourier transform, Frequency analysis, Isotropy, Trabecular bone

Subject Categories

Computer Sciences | Other Computer Sciences

Frequency Analysis Of Trabecular Bone Structure

A Thesis

Presented to

the Faculty of the Daniel Felix Ritchie School of Engineering and Computer Science

University of Denver

In Partial Fulfillment

of the Requirements for the Degree

Master of Science

---

by

Daniel Parada San Martin

November 2022

Advisors: Haluk Ogmen & Mario Lopez

Author: Daniel Parada San Martin
Title: Frequency Analysis Of Trabecular Bone Structure
Advisor: Haluk Ogmen & Mario Lopez
Degree Date: November 2022

Abstract

Medical data is hard to obtain due to privacy laws making research difficult. Many databases of medical data have been compiled over the years and are available to the scientific community. These databases are not comprehensive and lack many clinical conditions. Certain type of medical conditions are rare, making them harder to obtain, or are not present at all in the aforementioned databases. Due to the sparsity or complete lack of data regarding certain conditions, research has stifled. Recent developments in machine learning and generative neural networks have made it possible to generate realistic data that can overcome the lack of data in the medical field. For example, the study of osteoporosis, poor bone density, or osteoarthritis, over abundance of bone material, has been studied extensively. Despite the commonality of these conditions, getting data is still difficult. This data is required to develop treatments but it is a problem that continues to plague an ever aging population. The ability to generate bone data with specific micro-structural parameters, enabling the simulation of real world data, for a desired medical condition would remove the high barrier that currently exists in the field.

This thesis explores fundamental properties of bone microstructure that can help describe said structure. This would provide insight into the bone spongiosa, the interior portion of bones, which contributes to bone stability. It explores the bone microstructure in the frequency space through the Fourier transform in order to explore useful properties, like isomorphism.

Keywords:

Micro-structural parameters, Frequency Analysis, Fourier Transform, Bone structure, Fractal Analysis, Isotropy

Acknowledgements

I would like to thank my advisors Haluk Ogmen and Mario Lopez for their guidance, patience and talking me out of rabbit holes I climbed into far too often.

I would also like to thank Cathy Durso for her patience in discussing statistics for days on end.

Table of Contents

1 Introduction **1**

1.1 Introduction . . . 1

1.2 Problem Statement . . . 2

1.3 Thesis Contributions . . . 3

1.4 Organization of Thesis . . . 3

2 Related Work and Background **4**

2.1 Fractal Analysis . . . 4

2.2 Denoising . . . 5

2.3 Trabecular Bone Anisotropy . . . 7

2.4 Fourier Transform Use in Bone Structure . . . 7

3 Data Description **10**

3.1 Bone Dataset . . . 10

4 Approach **15**

4.1 Data Preprocessing . . . 15

4.1.1 Packages/Technologies . . . 16

4.1.2 Approach . . . 16

4.1.3 Discussion . . . 16

4.2 Fourier Transform of the Data . . . 17

4.2.1 Fast Fourier Transform . . . 17

4.2.2 Packages/Technologies . . . 18

4.2.3 Method . . . 18

4.2.4 Discussion . . . 19

4.3 Magnitude Spectrum Visualization . . . 19

4.3.1 Packages/Technologies . . . 20

4.3.2 Method 20
4.3.3 Discussion 24
4.4 Circularity Index Metric 24
4.4.1 Packages/Technologies 25
4.4.2 Method 26
4.4.3 Discussion 30
4.5 Statistical Analysis 31
4.5.1 Packages/Technologies 31
4.5.2 Method 31
4.5.3 Discussion 33

5 Conclusion and Future Work **34**

Bibliography **35**

List of Figures

3.1 Sample patch (modified from [6]) 11
3.2 Isotropic example 12
3.3 Isotropic magnitude spectrum 12
3.4 Quasi-Isotropic texture example 13
3.5 Anisotropic texture example 14

4.1 Original bone sample (left) and the grayscale version (right). 15
4.2 Bone and Magnitude Spectrum 17
4.3 Bone sample 45 degree rotation 20
4.4 Example of a "slice" of the magnitude spectrum 21
4.5 Slice with large frequency radius 22
4.6 Multiple sample slice 23
4.7 Small magnitude frequency slice 23
4.8 Barycenter of frequency distributions 25
4.9 Quasi-circular (left) and non-circular frequencies distributions 26
4.10 Circularity index with error bars (standard error of the mean) 28
4.11 Circularity index close-up 29
4.12 Wavelength scale on a sample patch 29
4.13 First and second dips in circularity index 30

1. Introduction

1.1 Introduction

The Health Insurance Portability and Accountability Act, or HIPAA, is a federal law that requires healthcare professionals to securely store and transfer patient information. This law requires that data transferred digitally be protected from data breaches, inconsistencies and that patient data be kept confidential. This results in patient medical records being kept private and can only be released or transferred with permission from the patient. This adds a considerable amount of red tape when trying to obtain medical data for studies. The scarcity of data can significantly slow down progress in medical research. This is further aggravated when dealing with rare medical conditions or conditions that may carry a stigma in society. Further aggravating data scarcity.

The Privacy Rule allows certain entities to use and disclose protected health information for research purposes. This can be done with individual authorization, or in certain cases without individual authorization but it is under limited circumstances. Individual authorization can be time consuming as each person must grant access to their medical information to the research entity. Often data must be limited or de-identified in order to be used for research to ensure the privacy of the people whose data is to be used. The de-identification of data is also a time consuming procedure as there are many variations and models of the medical equipment used in hospitals to obtain or diagnose similar conditions. Something as simple as an X-ray of a broken bone can have identifying patient data in the X-ray itself and the placement is not consistent across all machines.

The aforementioned data scarcity and imbalance problems can be addressed by generating artificial data. One approach for data generation is through machine learning.

For example, generative neural networks, which consist of two neural networks trained simultaneously, one which is trained to generate a specific type of data and another which is meant to detect fake and real data apart through inconsistencies in characteristic properties of real data. An alternative approach is to generate data based on known properties of the real data. For example, if we know the statistical properties of noise in the data, we can generate several versions of data by resampling the known noise distribution and thereby generating multiple realizations of the noisy data.

There is a wealth of research into diseases that have plagued humanity since the dawn of civilization. Throughout history the medical advancements have steadily increased the life expectancy of people around the globe. However, with every disease that is conquered or at the least controlled, there is always a new threat looming over the horizon. As the human population expands so does our exposure to novel diseases. In some cases, these diseases can cause a premature breakdown of our bodies. Osteoporosis is one such condition triggered by the aging body as our bones decrease in density. This makes senior citizens particularly susceptible to fractures. As the general life expectancy increases, so does the prevalence of these age-related diseases in the population. This in turn leads to increased health-care costs and decreased quality of life.

1.2 Problem Statement

Osteoporosis research uses images of healthy and diseased bones in order to analyze the genesis and the progress of the disease as well as to determine the efficacy of treatments. Given the limited nature of bone images, it is highly desirable to create artificial data that reflect accurately the properties of human bones. One approach for data generation starts with a small bone-structure sample (called bone micro-structure) and "grows" this sample to obtain larger bone images [12].

A key problem in this approach is to determine how to grow the sample in different spatial directions. If bones are isotropic, the growth should take place similarly along all directions. On the other hand, if bones are not isotropic, then the growth process should take into account anisotropic properties of bones. The goal of this thesis is to analyze bone images in order to determine if bones have isotropic properties and at which scale do we observe that type of structure.

1.3 Thesis Contributions

The following work looks to make meaningful contributions to the study of bone microstructure in the frequency domain and perform statistical analysis to verify their significance. This is done with the goal of resolving the scarcity of healthy bone data through the study of bone micro-structural parameters in the frequency domain. Such an addition can prove useful in the artificial generation of bone microstructure through a better understanding of bone properties in the frequency domain.

Over the following sections the approach to identify key characteristics of bone microstructures will be discussed at length. Results obtained will be analyzed through statistical analysis in order to ensure that results are consistent with bone data at large rather than being the result of small edge cases. Statistical significance of results will be established.

1.4 Organization of Thesis

This thesis is structured into the following chapters:

- Related Work and Background : This chapter explores existing and relevant contributions on the study of bone spongiosa micro-structure, and frequential analysis of bone. It covers some of the basic theoretical notions. Imaging technologies, imaging processing, fractal parameters, and challenges in the field are discussed.
- Data Description : In this chapter the data, its collection and its handling is discussed in the scope of this study.
- Approach Discussion : This chapter discusses the multiple approaches, goals and processes developed in the study of bone micro-structure and its characteristics. It will also discuss the robustness of the approach.
- Conclusion and Future Work : In this chapter the results are summarized and discussed. We will also discuss possible avenues to explore in future work so it can serve as a guide moving forward.

2. Related Work and Background

This section will discuss the most recent approaches in the study of spongy bone micro-structure, including methods of acquiring bone data, the processing of this data and parameters found to be of interest.

2.1 Fractal Analysis

Studying spongy bone microstructure of human vertebrae in-vivo is called quantitative computed tomography (QCT). This is useful when studying certain medical conditions like osteoporosis, loss of the spongy microstructure of the bone, which increases the risk of fracture. In assessing bone quality there are certain parameters of interest like bone mineral density (BMD), turnover rates, micro architecture, mineralization and damage accumulation [3]. Among these parameters of interest, BMD alone is able to account for roughly 70% of variability of the failure load, amount of force required to fracture the bone, while all other parameters contribute far less. However when data is noisy, more robust algorithms are needed to compute the risk of fracture in vertebrae.

A fractal approach has been suggested [12] which proposed five fractal parameters which together circumvent current limitations of other methods like explicit skeletonization of the trabecular bone and well defined transitions between bone and marrow [2]. The fractal method is able to introduce new parameters from QCT which are robust to noise, helps in determining overall bone strength and has relations to existing microstructural parameters. These parameters were able to show correlations between trabecular thickness and rod volume/bone volume with the respective trabecular thickness and structure model index. It is a method that has been shown to be more robust to noise for in-vivo data than pre-existing methods.

2.2 Denoising

Computational Tomography (CT) scans are prone to noise just like any other forms of signal acquisition. There are certain physical phenomena that are inherent to the method of acquiring the CT scan; however, there is a plethora of techniques that can be employed to correct such issues. When a CT scan image is being generated, the machine that obtains the image commonly uses an iterative reconstruction process which helps deal with noise.

Several techniques that exist for CT image reconstruction are discussed in [11], including :

- Filtered Back Projection (FBP) : is based on multiple assumptions in order to simplify CT geometry, compromising between image noise and reconstruction speed. It has been the default reconstruction technique for decades.
- Adaptive Statistical Iterative Reconstruction (ASIR) : makes more complex assumptions about the CT geometry along and through multiple iterations of reconstruction it achieves less image noise but has a slightly longer reconstruction time.
- Model-based iterative reconstruction (MBIR) : uses detailed models of several of the characteristics of radiation and CT equipment. It uses backward and forward projections to match the reconstructed image to a statistical metric of the acquired data. This study employed two independent blind reviewers to analyze the CT scans of 36 patients totaling a known number of 51 liver lesions. Whilst the reviewers managed to identify and categorize all of the liver lesions without any statistically significant differences, it was noted that the CT scans that used model based iterative reconstruction (MBIR) were less noisy. The mean lesion contrast to noise ratio was significantly higher for the MBIR algorithm than for the FBP and ASIR.

Despite the differences in processing speeds: 15 images/second (FBP), 10 images/sec (ASIR) and 1 image/sec (MBIR), with the ever improving computational capabilities of newer CT scans the improvement in image quality versus reconstruction speed is well worth the benefits.

Given that a multitude of noise sources for CT images exist due to physical and statistical uncertainty, a review of the different sources was conducted by Diwakar et al. [4].

There are certain sources for noise such as metal artifacts, patient motion and round-off errors which cannot be changed through software after the fact. On the other hand, there are certain sources noise that we can work with to improve image quality like beam hardening (increase in average energy of X-ray that passes through the patient) which is statistical noise and random noise which also comes from the X-ray quanta used to generate CT images (it presents as a change to image density). To deal with these noise sources, several techniques were discussed in the paper such as Wavelet transform, intra and inter scale dependencies and block- matching and 3D filtering (BM3D). The purpose of all of these techniques is to obtain a piece-wise constant, or slowly varying signal in homogeneous tissue regions while maintaining sharp boundaries. Out of all of the methods mentioned in the article not a single one proved to be the "best" when it came to noise reduction, as each had its advantages and disadvantages and it is clear that there is a trade-off between edge preservation and noise reduction.

The advancements in computational power and the rise of convolutional neural networks were employed by Thomsen et al. [13] to produce a noise reduction filter based on a 3D convolutional neural network with the goal of computing micro-structural parameters, such as tissue mineral density, bone volume/total volume and bone mineral density, with better accuracy. This new method was compared to state-of-the-art wavelet-based noise reduction techniques as well as to a standard neural network. The convolutional neural network outperformed both. It improved the computation of certain micro-structural parameters whilst avoiding over-fitting the data used for training.

In all studies, having more data leads in general to better results; just as important though is the quality of the data available. A deep learning based algorithm was employed in Guha et al. [5] to obtain high-resolution reconstruction of trabecular bone from low-resolution CT scans using GAN-Circle. Due to the ever evolving technologies employed in CT scanners, there can be a large discrepancy between imaging facilities. Employing a GAN-CIRCLE algorithm was shown to help in data harmonization due to differences in equipment. Trabecular thickness was measured in true high and low resolution CT scans, and reconstructed high and low resolution CT scans. It showed that self-similarity score between measurement were significantly improved over the use of low resolution CT scans. Employing such a technique could prove useful when conducting studies that use data from different facilities or same facilities at different times.

Modified autoencoders have been proposed [7] in order to handle the injection of noise at the input level and in the stochastic hidden layer, which experimentally found that denoising variational autoencoders (DVAE) yielded better log likelihood than standard VAE. This implementation showed that it is possible to learn more robust and flexible approximate posterior distributions like mixture of Gaussian than the standard approaches.

2.3 Trabecular Bone Anisotropy

The study of bone trabeculae and it's primary direction has been studied with varying degrees of success. A paper by Ketcham et al. [10] discusses three methods for quantification of anisotropy in bone. They examined mean-intercept length (MIL), star length distribution (SLD) and star volume distribution (SVD) in 3D data. Using the directed secant algorithm, frequently used for traversing pixel and voxel grids to estimates the aforementioned quantities, is prone to bias. The paper discusses a possible normalization which helps in reducing the bias of the algorithm but still found that systematic divergences in the results occur due to the data used and its preprocessing. This impacts the ability to estimate the mechanical properties of the bone.

The ability to reproduce natural bone with complex structure and properties can be achieved using porous bone substitutes. A study found a numerical method for anisotropic evaluation of micro-structures [9]. This approach used a generalized Hooke's law and finite element method, dividing a volume into small units of that volume. It was shown that it is possible to characterize the spatial distribution of the modulus and anisotropy. The modulus anisotropy was dependent on the distribution of material and response mechanisms of modulus spatial distribution.

2.4 Fourier Transform Use in Bone Structure

It is commonplace to transform data in order to obtain new insights into underlying or defining characteristics of the data. A common data transformation technique is the use of the Fourier transform, typically through the application of the Fast Fourier Transform (FFT) algorithm. This technique translates data from the spatial domain to

the spatial-frequency domain. As mentioned in the previous section, the Fourier Transform has been used as a tool to investigate isotropy property of bones through visual inspection and dispersion indices. In this thesis, we propose an automated method for examining isotropic properties of bones.

The Discrete Fourier Transform (DFT) is computed using the FFT algorithm. This decomposes the input signal (image) into sine and cosine functions. The relationship between the sine and cosine functions can be expressed using the complex exponential function. The real part of the function corresponds to the cosine function and the imaginary part to the sine function. As noted before, the image is decomposed into a series of sine and cosine functions and can be expressed as follows for an image of size$N \times N$:

$$F(u,v) = \frac{1}{N^2} \sum_{x=0}^{N-1} \sum_{y=0}^{N-1} f(x,y) \times e^{-2j\pi(\frac{ux}{N} + \frac{vy}{N})} \tag{2.1}$$

$$F(u,v) = \frac{1}{N^2} [\sum_{x=0}^{N-1} e^{-2j\pi\frac{ux}{N}} \times \sum_{y=0}^{N-1} f(x,y) \times e^{-2j\pi\frac{vy}{N}}] \tag{2.2}$$

This can be simplified into :

$$F(u,v) = Re(F(u,v)) + jIm(F(u,v)) \tag{2.3}$$

where the real part of the expression, Re(F(u,v)), corresponds to the cosine function and the imaginary part of the expression, Im(F(u,v)), corresponds to the sine function. This representation is a polar coordinate transformation where each sine/cosine pair is specified by a corresponding magnitude and phase. The magnitude is the square root of the sum of the squares of the real and imaginary parts of F(u,v) and describes the image in terms of the amplitudes of its sinusoidal components. The phase is given by $arctan\frac{Im(F(u,v))}{Re(F(u,v))}$ and describes the relative positioning of the sinusoidal components in the image. In this work we will concentrate on the use of the spectrum of the FFT. Our focus is in the structure of the bone and not its relative location.

Josso et Al. [8] proposed a method for calculating the angle of a texture and degree of anisotropy. By computing the Fourier transform of an image the algorithm characterizes the distribution of the spectrum around zero frequencies by PCA. This results in the orientation and index of confidence on whether the texture is oriented (anisotropic or not).

Using the PCA method for the texture orientation, the index of confidence expresses if the texture is isotropic or not. A 0% confidence means that the texture is isotropic and 100% means a strongly anisotropic texture.

The degree of anisotropy (DA) of bones is determined by the bone microstructure. It has been proposed to study the anisotropy of bones [1] using calcaneus radiographs and the Fourier transform (FT). The spectra of the FT shows the vertical and horizontal components corresponding to the transversal and longitudinal trabeculae. This approach was based on a visual inspection and measurement of the spreading angles : Dispersion Longitudinal Index (DLI) and Dispersion Transverse Index (DTI). These were used to compute the DA. Synthetic images with varying degrees of anisotropy were generated and two observers analyzed the FT spectra with 1.5% and 3.1 % for intra-and inter-observer reproducibility, respectively.

3. Data Description

In this chapter we describe the sampling procedure for the available data, and design of the analysis of the data.

3.1 Bone Dataset

The data used in this study comes from the MICCAI 2020 paper [6]. This dataset is composed of twelve human vertebrae (T12 and L1) which were embedded into epoxy resin. These vertebrae were transformed into cylindrical vertebrae phantoms. The phantoms were then scanned using a high-resolution peripheral QCT (HRpQCT) using an isotropic resolution of 82 pm, 59.4 kVp and 900 pAs (XtremeCT I, Scanco Medical AG, Bruttisellen, Switzerland). The kiloVoltage (kVp) is the peak potential applied to the tube which increases the x-ray emission spectrum. The picoampere seconds (pAs) is the tube current which affects image quality. A review of Ct scan technical specifications can be found in [4]. The density values were automatically calculated. The spongiosa, where the trabeculae are located, was peeled from the cortex using a semi-automatic procedure and down-sampled to an isotropic resolution of 164 pm, which increased the signal-to-noise ratio which also reduced the voxel number per patch but managed to maintain most structural information.

A total of 7660 purely spongeous patches were defined on the entire set of vertebrae. These patches have an isotropic size of 32^3 voxels, which is a diameter of 5mm, and defined a regular offset of 8 voxels in all directions (1.3 mm). Figure 3.1 shows one of these patches. Patch densities were normalized from 31-350, 1100 mg/cm to [-1,1]. A cross section was taken from each voxel resulting in 7660 flat cuts of the trabeculae which were then randomly sampled and grouped into eleven distinct groups used in this study. This grouping was done in order to guarantee that sufficient data points were

available to establish a meaningful pattern for the data. The choice was made to work on 2D representations of these patches rather than 3D to simplify the study of the bone microstructure.

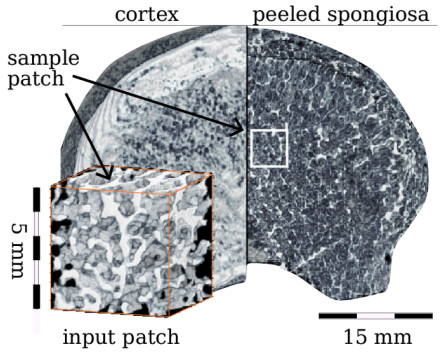

Figure 3.1: Sample patch (modified from [6])

The primary analysis being performed on this data will be carried out in the frequency domain. This transformation of the data from the space to frequency domain can yield interesting properties about the structure of the trabecular bone that makes up the core of bones. This transformation is to facilitate the detection of certain patterns in the frequency domain which will shed some light on physical characteristics of the bone. One such characteristic would be having an isotropic structure, identical change in certain properties regardless of the direction.

Prior to discussing the bone data directly let's first look at three examples of an isotropic texture, a quasi-isotropic texture and an anisotropic texture. Fig 3.2 is an example of a perfectly isotropic image: The pattern is the same in all directions: The concentric circles are all equally spaced and centered in the middle of the image.

Once we apply the Fourier transform to the isotropic image we obtain the spectrum and the phase of the image. We visualize the magnitude of the spectrum in Fig 3.3. Taking into account the fact that the concentric circles are equally spaced, the magnitude spectrum shows a circle whose radius corresponds to the isotropic frequency of the circles in the original image. The frequency is simply the inverse of the spacing of the circles in the original image. As illustrated in this example, spatial isotropy expresses

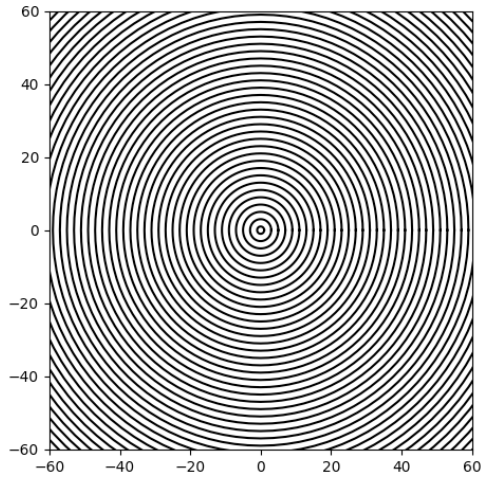

Figure 3.2: Isotropic example

itself as a circular structure in the Fourier Transform and the radius of the circle indicates the corresponding frequency. In a more complex image, there could be multiple frequencies at which isotropy occurs.

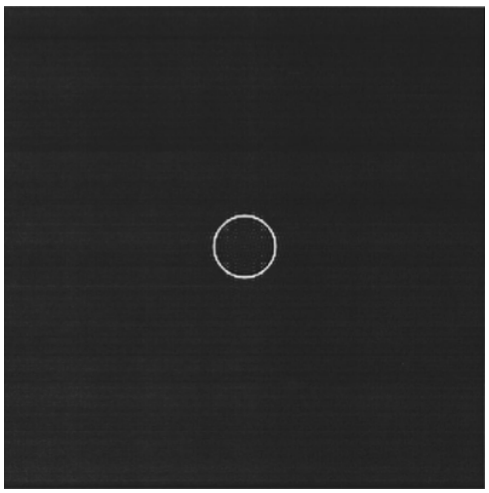

Figure 3.3: Isotropic magnitude spectrum

Figure 3.4 (left) is an example of a quasi-isotropic texture. It is a close up photo of a bar stool cover. When inspecting the image we can see that the fibers that make up the cover have a chess-board pattern with identical square-waves along the horizontal and vertical directions. Periodic patterns can be observed along other directions, but their

frequencies are not the same as the horizontal and vertical frequencies. The image and the magnitude spectrum are of identical size.

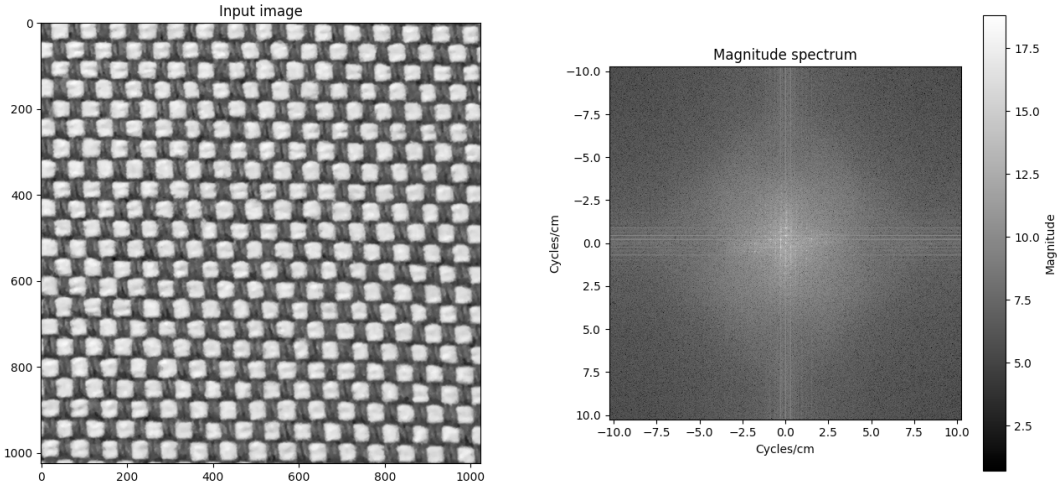

Figure 3.4: Quasi-Isotropic texture example

If we look at Figure 3.4 (right) we can see the corresponding magnitude spectrum of the image. The center of the spectrum represents the null frequency, i.e., the average luminance of the image. The x and y axes represent the spatial-frequencies with the low frequencies in the center and the higher frequencies towards the edges of the graph. The frequencies increase radially from the center from low to high. The areas of the plot which are lighter represent frequencies with a larger magnitude, i.e. more present in the image, and the darker regions have frequencies which are less prevalent in the image. First, as expected, we see the same pattern along the vertical and horizontal axes, reflecting the isotropy of the original image along these directions. As frequencies along other directions are different, the diamond-like shape of the spectrum shows us that the image is not completely isotropic. This result confirms the quasi-isotropic nature of the image; furthermore, we can see the directions in which we have the isotropic property.

For Figure 3.5 (left) it is a close up photo of a dresser made of wood. In this case, we can clearly see that the wood grain has a primary direction along the horizontal axis which makes this an anisotropic object. If we look at Figure 3.5 (right) we can see the corresponding FT magnitude spectrum. Similar to the isotropic and quasi-isotropic images above, lighter regions represent frequencies with a larger magnitude and darker regions

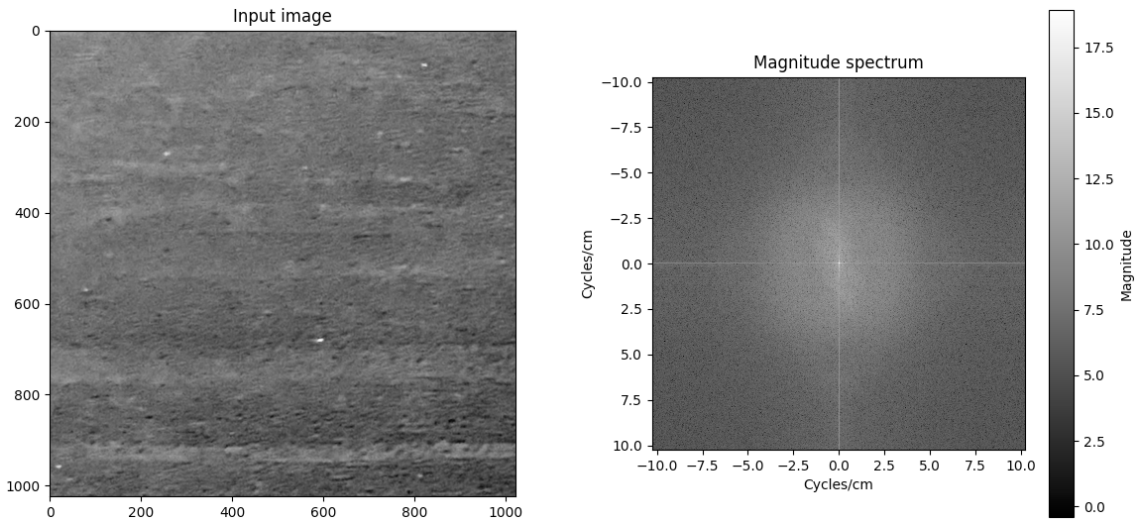

Figure 3.5: Anisotropic texture example

have frequencies which are less prevalent in the image. The spectrum shows a vertical orientation, reflecting the periodicity along the vertical dimension of the original image (resulting from repetitive horizontal "lines" in the image).

In summary, a circular structure in the spectrum indicates perfect isotropy. Whilst we can easily detect whether or not a pattern is isotropic or not with the naked eye while looking at simple images, like the concentric rings, chess-boards, it is much harder to do so on more complex images like those of trabecular bones. In addition, detecting whether isotropic properties are present is not enough but we must also know at which scale, frequencies, this isotropic property holds. At a small enough scale objects may appear isotropic, for example a close up of a line drawn with a pencil. When looked at from a very close distance the graphite left by the pencil can seem like random flakes but when looked at a larger scale it will be obvious that the line drawn with the pencil will be anisotropic. In this thesis, we will use a computational approach to determine isotropy. We will assess circularity in spectra by fitting circles and assessing the goodness-of-fit.

4. Approach

In this section we will discuss the approaches explored and the selection of the pipeline based on the desired outcomes, complexity and robustness. The goal will be to give a clear explanation of the steps taken in our approach that gives us additional insight into bone microstructure of the trabeculae bone that can be used to move research forward.

4.1 Data Preprocessing

The data set is composed of images retrieved from the voxels of the CT scans and have dimensions of 5mm×5mm. These images are read into the program containing the three color channels of a typical RGB image which, through a linear combination, are then averaged to form a one color channel. The resulting image is a 2D numpy array with floating point values which correspond to the grayscale of the images. The image in Fig. 4.1 is one sample of the data set used which shows the microstructure of the spongy bone inside of a human vertebrae.

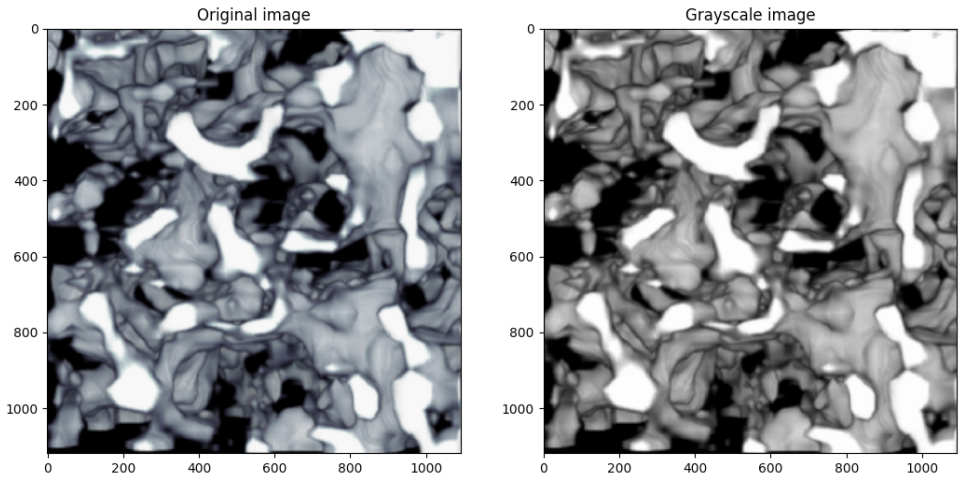

Figure 4.1: Original bone sample (left) and the grayscale version (right).

4.1.1 Packages/Technologies

The images used required pre-processing prior to performing any analysis. The images used contain 3 channels for RGB which needed to be transformed into a grayscale image. In order to transform the images into grayscale images, the Numpy[1] package was used to store the image resulting in a 2D numpy array. The original image is multiplied by a weight vector using the dot product resulting in a single value per pixel corresponding to the grayscale value. The weights used for the red, green and blue channels are 0.2989, 0.5870, 0.1140 respectively. Notice that the green value is much higher than red and blue, this is based on research performed on the human eye and its ability to perceive more shades of green than any other color. The transformation of the data results in a 2D numpy array containing floating point values which correspond to the grayscale level of each pixel in the image (Fig. 4.1).

4.1.2 Approach

In order to analyze the database of images, which are now composed of 2D numpy arrays representing the grayscale images, a preliminary analysis of single images was carried out. Images were chosen randomly, transformed into grayscale images and transformed from spatial representation to spatial-frequency representations. For this study, we focused solely on the magnitude of the FFT spectrum of the data. This sampling of the data was performed in order to observe the structure of the magnitude spectrum of the bone. This preliminary study is used in a later section to determine the range of possible values of the magnitude of the spectrum. We will investigate circularity for different values of the magnitude and determine spatial frequencies corresponding to circular, i.e., isotropic, structures.

4.1.3 Discussion

Given the transformation of the images, it is possible to modify the function used to transform the images into grayscale. The function is a rather simple weighting function. It takes in the values from the red, green and blue channels and assigns each color a weight and performs a linear combination of all three. The weights that can be used varies but literature suggests the weights used for this project mentioned above.

[1] https://numpy.org/

4.2 Fourier Transform of the Data

A brief theoretical background on the FFT is given in section Fourier Transform Use in Bone Structure. It explains the transformation of data from the space domain to the spatial-frequency domain.

4.2.1 Fast Fourier Transform

For this study, only the magnitude of the FFT transform will be used. This is because our main focus is on the bone microstructure rather than its relative location in the data. Furthermore, we will use the magnitude of the spectrum in order to properly quantify the frequencies that make up the bone. We will also take the log of the magnitude of the spectrum in order to improve the dynamic range of the values we observe.

Having discussed the mathematical equations of the Fourier Transform from the space domain to the spatial-frequency domain 2.1, let's see what the transformation looks like for a bone sample. In Figure 4.2 we can see a bone sample (left) and the corresponding magnitude spectrum of the Fourier Transform (right) after having been preprocessed into a grayscale image. The grayscale values are given on the image to show the intensity for the bone image on the left and the magnitude of the Fourier components on the right.

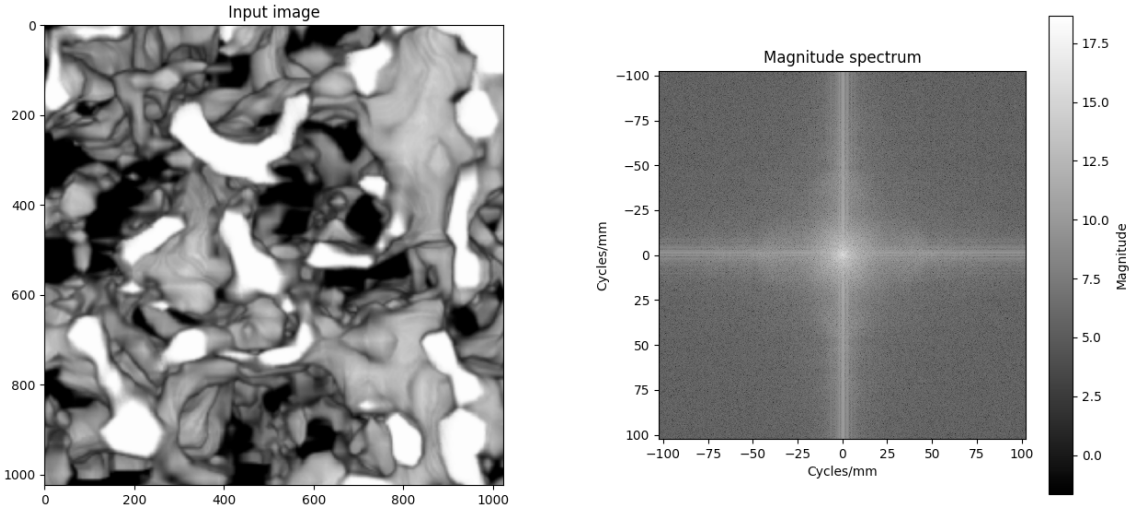

Figure 4.2: Bone and Magnitude Spectrum

We can clearly see multiple features on the magnitude spectrum's graph (right). Vertical and horizontal lines can be clearly seen, as well as several lighter clusters along the lines. Also near the center a more circular light shape can be seen. The lightness of these features represent the magnitude of the frequencies in the image. The lighter the feature, the more present a certain frequency is in the image.

4.2.2 Packages/Technologies

The Fourier Transform is a well known algorithm that has been implemented in a myriad of python libraries. Given that all implementations accomplish the same task in a comparable amount of time, the Numpy FFT [2] version was chosen for this study. Similarly the absolute value and log functions from the Numpy library were used.

4.2.3 Method

Fourier Transform is a mathematical decomposition of functions that depend on time/space into functions that depend on frequency. The application of the Fourier Transform on a 1D signal, such as sound, expresses the signal in terms of the frequencies that make up that specific sound. The 2D Fourier Transform is an extension of the 1D Fourier Transform which takes the Fourier Transform along the columns first and then along the rows. This decomposes the image into the different frequencies that define the image. Both of these steps are carried out sequentially by the 2D FFT in Numpy.

Taking a closer look at Figure 4.2, we can begin to interpret some of the features mentioned above. Starting with the bright horizontal and vertical lines, they correspond to the vertical and horizontal, respectively, edges that are present in the bone sample. Something that we can easily verify by inspecting the image.

Along the horizontal and vertical lines, we can also see small lighter regions corresponding to large magnitudes. Since these regions are clustered around the horizontal and vertical lines, they correspond to frequencies present in the image with a primary direction. This means that it shows anisotropic bone structure at these frequencies. The last thing to note on the magnitude spectrum is the area of the graph around the center.

[2] https://numpy.org/doc/stable/reference/generated/numpy.fft.fft2.html

We can clearly see a lighter region with a circular shape. This corresponds to potential isotropic bone properties at these frequencies.

4.2.4 Discussion

Looking at a single example we can see that the magnitude of the spectrum can be easily interpreted and provides some insight into the makeup of the bone microstructure. It is clear that the bone contains certain frequencies that have a primary direction, patches along lines which corresponds to anisotropy. Whilst there are others that show more isotropic properties like the circular lighter patch in the center of the magnitude spectrum.

Visually inspecting and analysing the magnitude spectrum for every image would not be efficient, nor particularly enlightening, and would be prone to errors and assumptions. Even ignoring those shortcomings, analysis through visual inspection would only provide a very broad view of the makeup of the bone structures. A more in depth analysis must be done on the magnitude spectrum so that we may retrieve a subset of frequencies corresponding to the isotropic properties of the bone structure. This task will be accomplished and discussed in the following sections of this chapter.

4.3 Magnitude Spectrum Visualization

An interesting observation we can make is that a rotation of the input image by an angle will result in a rotation of the magnitude of the spectrum by that same angle. We can clearly observe this phenomenon in Figure 4.3. The image and magnitude spectrum on the left correspond to the 45 degree rotation, and the magnitude spectrum and image on the right correspond to the original image.

The rotation is very apparent for the horizontal and vertical lines. By applying a rotation of 45 degrees to the input image we obtain a magnitude spectrum that is also rotated by 45 degrees. Performing this rotation confirms that the transformation from the space domain to the frequency domain decomposes the input image into the frequencies with the correct orientations. When we rotate the original image, it results in cropping the image. This is why the rotated image is zoomed in on the bone structure in Fig 4.3.

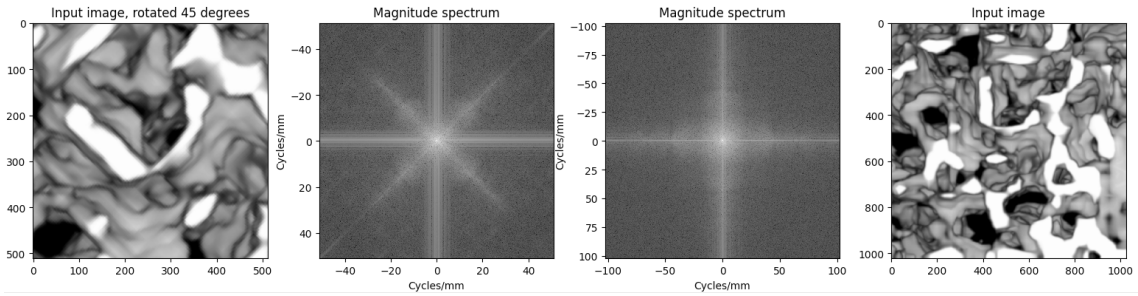

Figure 4.3: Bone sample 45 degree rotation

Let us revisit the magnitude spectrum of the example given in Figure 4.2 (right). As we discussed previously, the magnitude spectrum represents the decomposition of the frequencies that make up the bone image. Since we are looking at the magnitude of the spectrum, the darker regions of the graph are frequencies with small magnitudes and lighter regions represent frequencies with large magnitudes. Through visual inspection it is easy to see areas that have frequencies with larger magnitudes, i.e. more prevalent frequencies in the bone image. We wish to know which frequencies may show isotropic properties of the bone.

4.3.1 Packages/Technologies

The visualizations of the magnitude spectrum and input images is done using Matplotlib pyplot [3]. The retrieval of the frequencies at different magnitudes, or "slices" as they are referred to in the following section, were obtained using the Matplotlib pyplot contour package [4].

4.3.2 Method

After examining multiple samples of bone data, similar to Figure 4.2, the average maximum and minimum of the magnitude of the frequencies in the magnitude spectrum were estimated. The minimum and maximum values of the magnitude spectrum were found to be -0.73912766 and 17.86087234, respectively. As a reminder, we take the

[3] https://matplotlib.org/3.5.1/api/_as_gen/matplotlib.pyplot.html

[4] https://matplotlib.org/stable/api/_as_/matplotlib.pyplot.contour.html

log of the magnitude of the spectrum in order to increase the dynamic range of the values to overcome the limitations of 256 gray levels. This means that negative values are possible if the magnitude of certain frequencies are less than 1. We take note that the minimum value obtained for the magnitude is negative.

We wish to study the distribution of the frequencies of different magnitudes, not just the maximum and minimum magnitudes. An iterative process was applied in order to determine an appropriate number intervals at which to study the distribution of frequencies. A total number of 87 intervals equally spaced intervals was found to have a good ratio between discretizing the frequency domain and running time. This results in gained insight into frequency distributions with reasonable computation time. Decomposing the magnitude spectrum into 87 intervals equates to looking at a "slice" of the magnitude spectrum that intersects all frequencies with the corresponding magnitudes. This is similar to creating a topographical map of a mountain, where a given altitude (magnitude) is considered, only the part of the mountain at the given height would be visible. Figure 4.4 shows what a slice through the magnitude spectrum looks like. This work will allow us to explore the distribution of frequencies which will allow us to identify which frequencies isotropic bone properties.

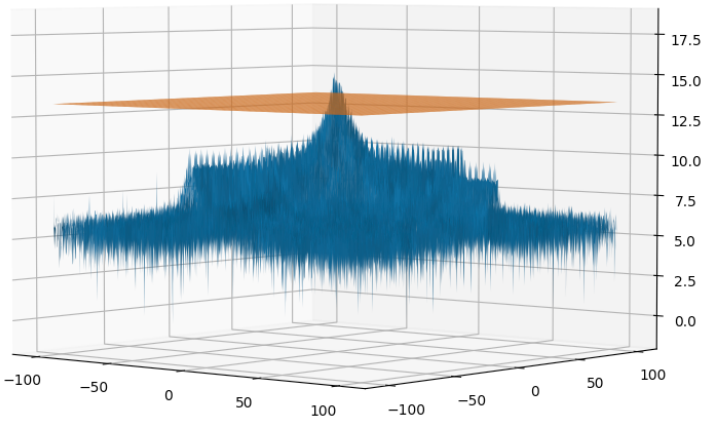

Figure 4.4: Example of a "slice" of the magnitude spectrum

Let's look at an example of a "slice" of the magnitude spectrum. Figure 4.5, shows the frequencies with magnitudes close to the maximum level previously found. These frequencies are represented by the blue dots. Given the distribution of the blue dots, we also plot the best fitting circle on the data points, centered in the barycenter of the

points. As mentioned in the previous chapter, the near circular distribution of points is indicative of isotropy and will be discussed further in the next section.

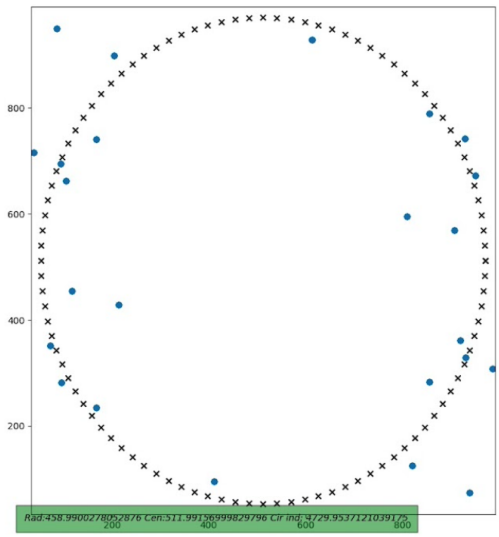

Figure 4.5: Slice with large frequency radius

This quasi-circular distribution of points can be observed in other samples of bone images. Figure 4.6 shows multiple data points from 3 separate bone samples. Each bone sample data point is marked using a unique symbol: dot, upside down triangle, and circle. Grouping a large number of bone samples when analysing the frequencies distributions we can ensure that the results represent the data in a meaningful way. This ensures that sufficient data points are available to be statistically significant.

The quasi-circular distributions observed in the two previous images are not observed for all magnitudes. Figure 4.7 shows the frequency distribution for multiple bone samples at a smaller magnitude slice. The distribution of the frequencies almost look that they contain asymptotes along the horizontal and vertical directions. Let's refer back to Figure 4.2, a complete magnitude spectrum figure. We can see that we have two light lines along the horizontal and vertical directions. The lightness of these lines represent large magnitudes. So when we take a slice of the smaller magnitudes, we get the darker regions of the magnitude spectrum which is what we see in Figure 4.7.

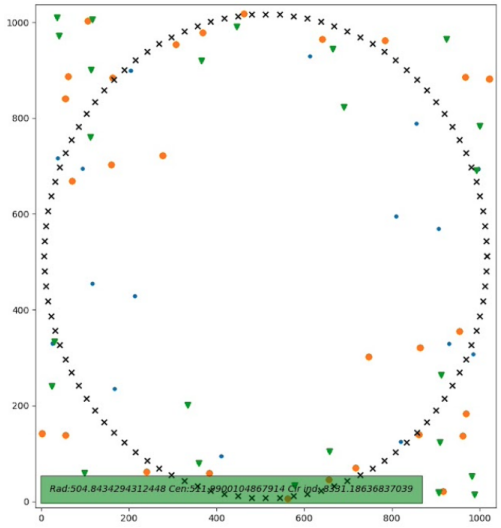

Figure 4.6: Multiple sample slice

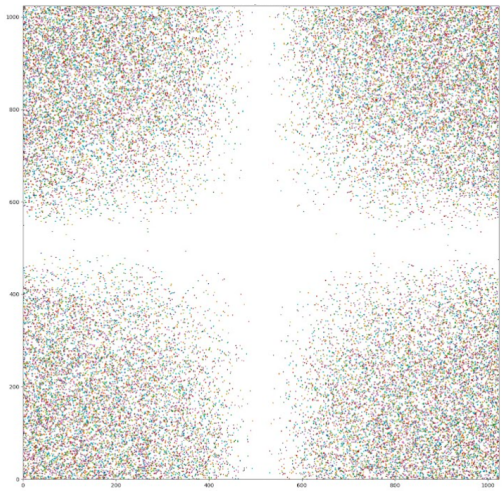

Figure 4.7: Small magnitude frequency slice

4.3.3 Discussion

In the previous sections, we explored two very distinct slices in the magnitude spectrum. For the larger magnitudes shown in Figure 4.6, a pattern begins to emerge. The quasi-circular distribution of the frequencies corresponds to a clear pattern in the bone microstructure that we can visualize in the frequency space. The frequencies that have the larger magnitudes correspond to the lighter lines in the magnitude spectrum and the center of the spectrum. The lines in the graph represent the edges that we see in the trabeculae and the lighter region in the center corresponds to the low frequencies. Further exploration and quantification of this pattern will be examined in the following section.

The second slice we explored (Fig. 4.7), contained no clear circular pattern that might indicate isotropy in the bone microstructure. The frequencies that were present in this slice correspond to the high frequencies in the image. High frequencies can represent noise, artifacts in the image with no clear pattern and edges of smaller bone structure. In future sections, we will examine the distribution of the frequencies at different magnitudes in order to identify circular patterns in the magnitude spectrum.

4.4 Circularity Index Metric

In the previous section, we observed the different distributions of frequencies based on the magnitude. For the larger magnitudes, we clearly identify a quasi-circular distribution of frequencies. A perfectly circular distribution of frequencies would mean that we have a perfectly isotropic object. This is because a circular distribution of frequencies translates to the same frequencies being present in all directions with equal prevalence (magnitude). It would be of great interest to be able to quantify this quasi-circular distribution in order to determine the level of isotropic structure of the bone and the scale at which the bone can be considered isotropic.

It is not enough to have a quasi-circular distribution of the frequencies to signify isotropic bone structure. The barycenter of the frequencies of each slice must be near the zero frequencies of the magnitude spectrum in order to establish a quasi-circular distribution of frequencies around the zero frequencies of the magnitude spectrum. Figure 4.8 shows a subset of the barycenters' distance to the zero frequencies of the mag-

nitude spectrum. The barycenter that is far from the zero frequencies belongs to one of the extreme slices.

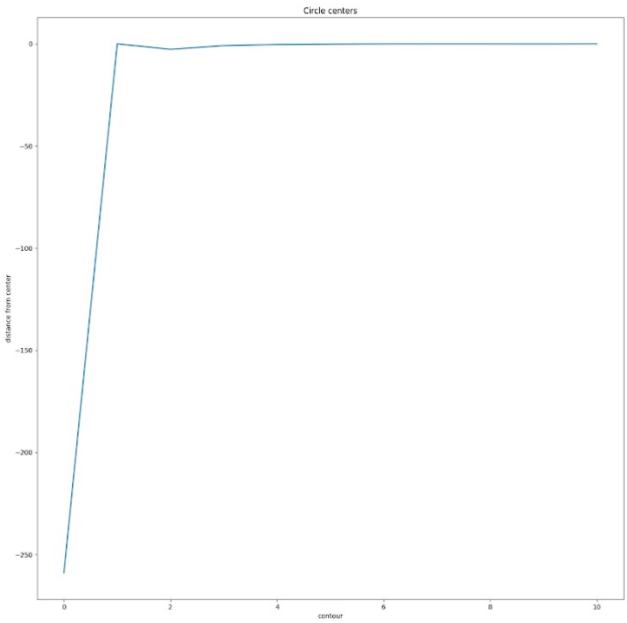

Figure 4.8: Barycenter of frequency distributions

This section will discuss the creation of a simple but effective circularity index used for the quantification of the frequency distributions at each slice. This results in an estimate of the isotropic properties of the bone for the frequencies present at each slice. We will discuss the steps in analysing the distribution of frequencies throughout the entire magnitude spectrum. The evolution of the circularity index will be explored and several points of interest will be discussed.

4.4.1 Packages/Technologies

In the creation of the circularity index, numpy and matplotlib libraries were extensively used. Numpy was used to obtain the minimum and maximum levels of the spectrum, compute the log of the values, circle centers for the best fitting circle and to determine the circularity index. Matplotlib was used in finding the contours, or points intersected for each slice of the magnitude spectrum. Finally the circle fit [5] library was

[5]https://pypi.org/project/circle-fit/

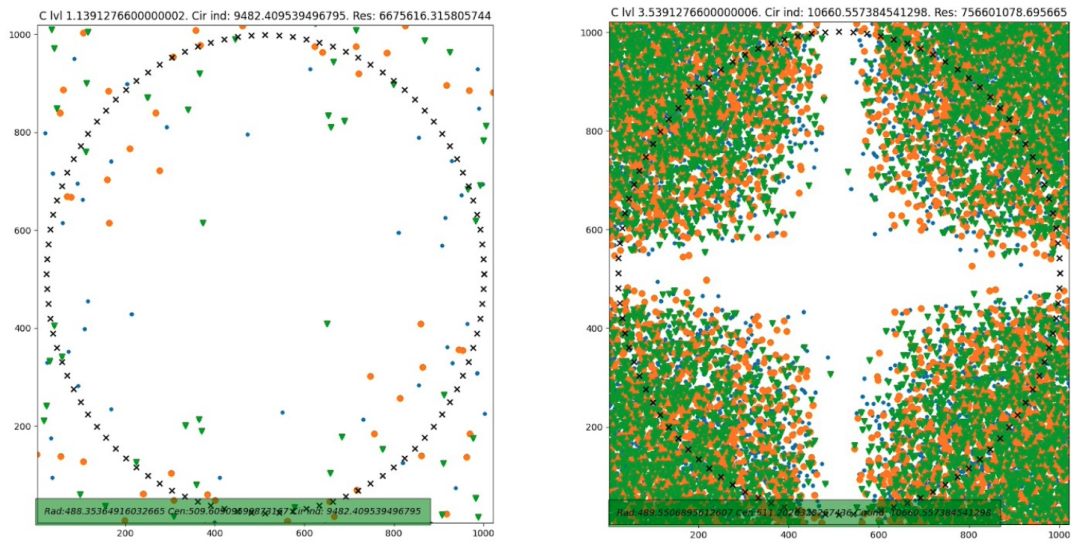

Figure 4.9: Quasi-circular (left) and non-circular frequencies distributions

used to generate the best fitting circle to the data points from each slice for which the circularity is analyzed.

4.4.2 Method

As discussed in the previous section, the bone samples were grouped into 11 distinct groups randomly without replacement. For each bone in every group, the Fourier Transform was computed. The logarithm of the absolute values of the resulting spectra were calculated along with the average minimum and maximum values of the magnitude spectra. This was followed by the computation of 87 equally spaced intervals at which the intersecting frequency distributions were studied. Two samples of these slices were shown in Figures 4.7 and 4.6. This process was applied to all images in all 11 groups of data, resulting in 87 slices in each of the groups. For each slice in a group, the best fitting circle was fitted onto the data points on that slice. This results in the graphs seen on Figure 4.9.

It is clear from Figure 4.9 that the frequencies on the slice on the left have a more quasi-circular distribution than the ones on the right. In order to quantify this quasi-circularity we define the circularity index. The circularity index is a non-dimensional parameter which measures the L2 distance between each point on the slice and the best fitting circle. We then normalize the distance by dividing the result by the number of

points on the slice. This results in the average distance between the frequencies observed and a circular distribution. We can define the circularity as follows :

$$CI = \frac{\sum_{i=1}^{n} \sqrt{\|\vec{p}_i - \vec{c}_i\|^2}}{n} \tag{4.1}$$

where p is the point's coordinates, c is the circle's closest coordinates to the point considered, and n is the number of points.

The smaller this average distance, or circularity index, the more isotropic the bone structure is on those frequencies. Figure 4.9 (left) shows that at the magnitude spectrum of 1.1391, we have a circularity index of 9,482.4. Meanwhile the magnitude spectrum of Figure 4.9 (right) shows that at the magnitude spectrum of 3.5391, we have a circularity index of 10,660.6. Knowing what the circularity index represents, we clearly see that the left graph has a more circular distribution than the one on the right and we can now quantify it.

Now that we have transformed all of the data and have quantified the quasi-circular distributions of frequencies, we can visualize them to explore potential isotropic bone structure in the frequency space. Figure 4.10 plots for each o the 11 groups of bone data the circularity index for each of the 87 slices of the magnitude spectra. This results in 11 lines, one for each group of data showing the circularity index of their corresponding slices. On the same plot we also have the average circularity index value across all groups with the error bars as the mean plus/minus 1 standard error of the mean (SEM).

Let's take a closer look at Figure 4.10. We can clearly see the 11 lines for each of the groups and the corresponding circularity index values. Note however, that not all lines start and end at the same location. This is because by taking the average minimum and maximum values of the magnitude spectrum to create the intervals (slices) there are certain images that will not have frequencies matching those extreme cases. The circularity index values for all groups seem to follow a similar pattern around the 89.72 to 92.2 cycles/mm, with the exception of group 6. When taking a closer look on Figure 4.11 we clearly there are large dips in the circularity index. These dips show that the frequencies exhibit a more quasi-circular distribution than other frequencies. This means that the bone microstructure contains isotropic properties at those frequencies.

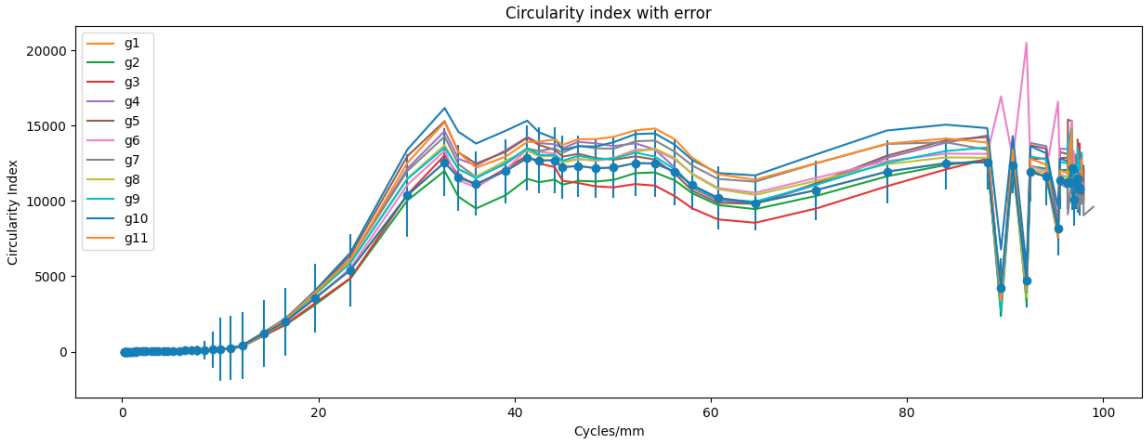

Figure 4.10: Circularity index with error bars (standard error of the mean)

If we examine Figure 4.11, we can see that the first of these frequencies of interest occurs at 89.72 cycles/mm. We convert from frequency to wavelength simply by calculating $\frac{1}{f}$. This results in a wavelength of 0.011 mm. The second of these frequencies of interest occurs at 92.2 cycles/mm. Similarly we compute the wavelength and obtain 0.0108 mm.

The average thickness of trabeculae bone in vertebrae is 0.16 mm. This means that the average trabecular thickness is around 10 to 12 times that of these wavelengths. This shows that the frequencies which exhibit isotropic properties correspond to the thinner trabecular bone that exists in the vertebrae. Figure 4.12 shows the scale of the wavelength computed from the frequencies of interest.

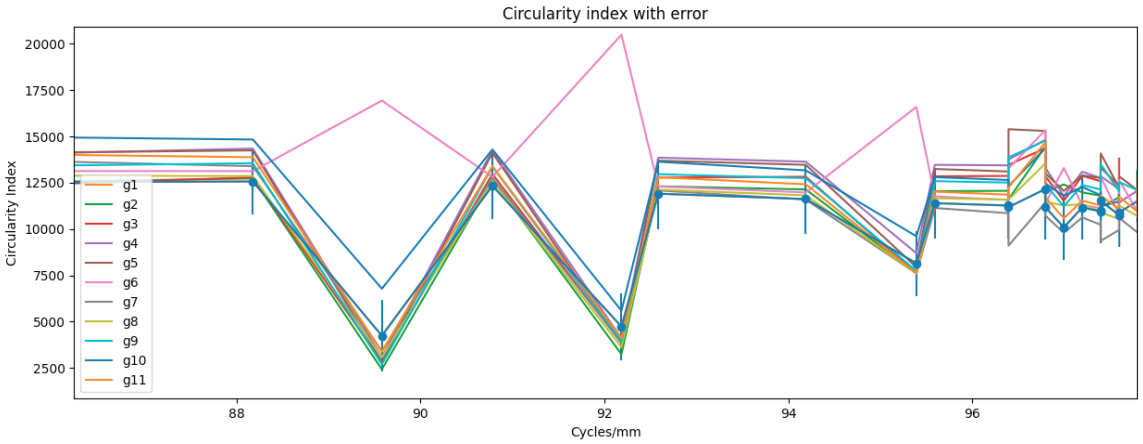

Figure 4.11: Circularity index close-up

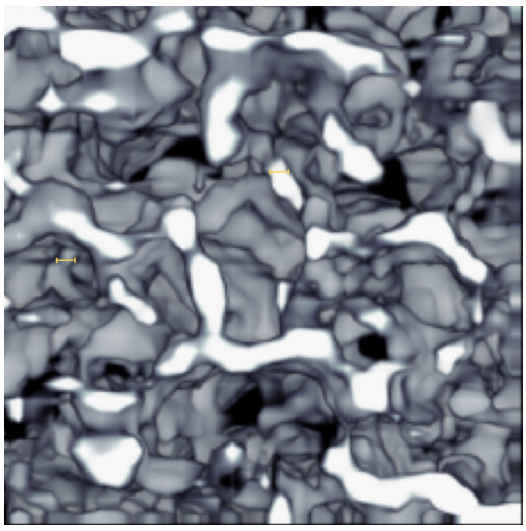

Figure 4.12: Wavelength scale on a sample patch

4.4.3 Discussion

Multiple dips in the circularity index were observed (c.f. Figure 4.11). The most pronounced dips occurred around frequencies 89.72 cycles/mm, 92.2 cycles/mm and 95.4 cycles/mm. Only group 6 did not exhibit these decreases in the circularity index. Every dip in the circularity index shows that for these frequencies have a more quasi-circular distribution than other frequencies in the magnitude spectrum. This directly translates to a more isotropic microstructure of the bone at these frequencies. Let's plot a closer look at both of these in Figure 4.13. From these figures we clearly see the similarity in the reduction of circularity index at the same frequencies.

We can observe that for all but two groups the circularity index is less 1 standard deviation away from each other (c.f. 4.11). We have successfully shown in this section, through the computation of the circularity index, that our application of the Fourier Transform has granted us insight into the bone microstructure. The consistency and scale of these dips in the circularity index allows us to establish a clear connection between frequencies and isotropic bone microstructure.

In Figure 4.12 we can clearly see the scale of these frequencies of interest. They correspond to the thinner trabecular bone that exist in our sample data. It shows that isotropic properties are present for the smaller scale trabecular bone that makes up the spongy portion of the vertebrae.

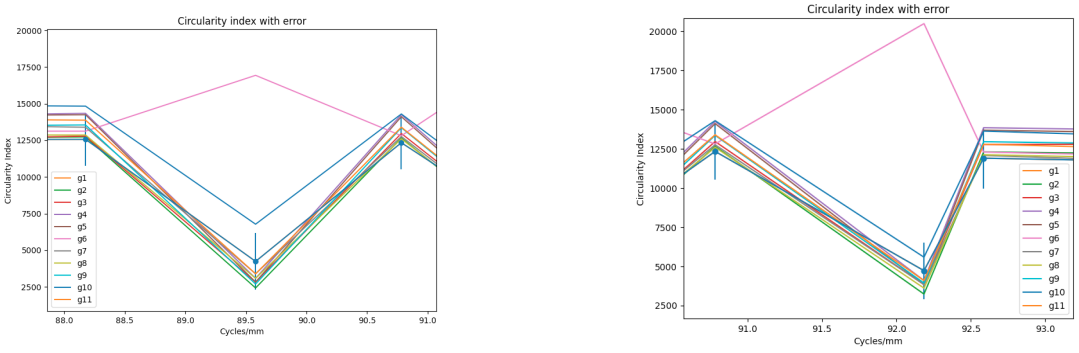

Figure 4.13: First and second dips in circularity index

4.5 Statistical Analysis

When observing the evolution of the circularity index on Figure 4.11 we must now answer the question : how significant are these decreases in values. Despite the sharp decreases in the circularity index values that we observed, we will determine if these decreases are statistically significant. The dip in all but one group must be looked at through statistics in order to determine the validity of the results. This chapter is consecrated to the statistical analysis of the behaviour of the circularity index.

4.5.1 Packages/Technologies

The stats package was used to compute the t-tests [6] carried out in this section. A Bonferroni correction was also carried out during the statistical analysis using Python's statsmodels library [7].

4.5.2 Method

In the previous section we looked at the evolution of the circularity index over the frequencies of the magnitude spectrum. Multiple decreases were observed for all groups but one, we now wish to verify if the dips are indeed significant. The decreases in circularity index are examined from low frequency to high frequency, i.e. left to right on Figure 4.11. A series of related t-tests are conducted on sequential data points for all groups in order to determine if there is a statistically significance increase or decrease in the circularity index values.

The first "significant" dip in the circularity index is observed around 89.72 cycles/mm. In order to determine if the dip is indeed significant we must verify if the circularity index values for 88.1 cycles/mm is significantly different from those at 89.72 cycles/mm (c.f. 4.13). This is accomplished by using a related sample t-test. This is commonly used in case-control studies or repeated-measures designs. Since we are measuring the circularity index for different frequencies of the same bone data we use the related sample t-test. This is a statistical procedure which determines whether the mean difference

[6] https://docs.scipy.org/doc/scipy/reference/generated/scipy.stats.ttest_rel.html

[7] https://www.statsmodels.org/dev/generated/statsmodels.stats.multitest.multipletests.html

between two sets of observations is zero. A standard p-value threshold of 0.05 is used to determine significance for this test. The difference in the circularity index value for the frequency of 88.1 cycles/mm and the circularity index for the frequency 89.72 were statistically significant. Resulting in a p-value of $5 * 10^{-5}$, well below our threshold. A related sample t-test was also performed between the circularity index value at 89.72 cycles/mm and 90.87 cycles/mm. This was done to determine if there was a statistically significant increase in the circularity index value. The difference in values was also statistically significant with a p-value of 6×10^{-5}.

We performed the same analysis for the second dip of the circularity index. The first data point, corresponding to 90.87 cycles/mm, and the second data point, corresponding to 92.2 cycles/mm, were statistically significant with a p-value of $5 * 10^{-4}$. For the second data point, corresponding to 92.2 cycles/mm, and the third data point, corresponding to 92.5 cycle/mm the difference in circularity index values are also statistically significant with a p-value of $9 * 10^{-4}$.

Given the results of the related sample t-test it seems that the result from the two large dips are indeed statistically significant. However ; the decreases in the circularity index values were not part of a previously formulated hypothesis we must correct for the large number of tests we performed on the data. The Bonferroni correction is a multiple-comparison correction method used when several dependent or independent statistical tests are performed on a data set. This correction ensures that we do not commit a series of type I errors. It corrects for this problem by lowering the α threshold value of the test performed, in this case the p-value, by dividing the threshold by the number of tests performed. In this study we perform a related t-test for every sequential pair of circularity index values, 87 data points for each group of the 11 groups. This results in roughly 946 related t-tests which means that the p-value threshold must be divided by roughly 1000. This makes our new threshold value be $5.3 * 10^{-5}$.

After performing the Bonferroni correction, we can verify the result from the first significant dip of the circularity index values remains statistically significant. The second significant dip in the circularity index values does not satisfy the more stringent threshold after the Bonferroni correction.

Another potentially interesting feature of the dip in circularity index would be symmetry in the increase/decrease of the circularity index, but no such characteristic was observed in a statistically significant way.

4.5.3 Discussion

In the previous section we visualized the evolution of the circularity index values and found multiple frequencies of interest. In this section, through statistical analysis, we verified that the frequencies that showed isotropic properties had statistically significant decreases in the circularity index values. By not having a hypothesis regarding the behavior of the circularity index values prior to studying the data, we performed a large number of related t-tests on all data points. Two frequencies of interest were identified and the related t-test applied to the data points around these frequencies confirmed that the decrease in the circularity index values are indeed statistically significant.

Due to the large number of related t-tests that were performed on the data, a more restrictive p-value threshold had to be set. This was accomplished through a Bonferroni correction, effectively dividing the p-value by the number of tests performed. After taking this correction into account, the first of the frequencies of interest maintained statistical significance. This shows that bone microstructure exhibits isotropic properties at given frequencies. This provides valuable insight into the spongy bone structure through a clear and concise algorithm.

5. Conclusion and Future Work

This research had set out to make a modest but meaningful contributions to the study of bone microstructure. In order to accomplish this, a large data set from the MICCAI 2020 paper [6] was used.

Through a preliminary exploration of the data we were able to inspect the spatial bone structure. This was followed by a transformation of multiple samples to the frequency domain through the use of the Fourier transform. An analysis of the frequencies that make up the bone microstructure was carried out using only the magnitude spectrum. The entire data samples were split into 11 groups with roughly equal number of samples. This was done to ensured that a large number of data points were available for the analysis carried out on the frequencies of the bone samples.

The circularity index, an adimentional metric for quantifying bone isotropic properties through frequency distribution analysis was introduced. By studying the evolution of the circularity index values, frequencies of interest related to isotropic bone properties were identified. These isotropic properties were found to be 0.011mm and 0.0109mm, roughly a tenth of the thickness of the trabeculae. We were able to visualize the scale of these wavelengths on a bone sample. It clearly showed the thinner trabecular bone corresponding to the 0.01 mm scale which exhibited isotropic properties. Finally, rigorous statistical analysis was done in order to establish that the results observed are indeed statistically significant. We took great care in ensuring that any bias that could have been introduced due to the large number of tests performed was taken into account.

Future application of this research could implement a study of the phase of the bone data as well as the magnitude spectrum. The information regarding relative position may prove useful in the relationships in spongy bone. Further work could also be done

in further exploration of the "slices" of the frequencies. A criteria can be defined for the circularity index which could warrant a more localized study of the frequencies that could be of interest. Some of this work was done during this research but proved to take considerable time to compute the more localized searches.

As mentioned in Section 3, it would also be possible to perform the analysis in 3D by applying the Fourier transform on the voxel rather than the 2D slice of the CT scans. The analysis for isotropic properties would require a frequency distribution that is spherical rather than circular. The "slices" of the magnitude spectrum would also have to be defined in 3D. It would also be interesting to apply this analysis to deceased bone, i.e. osteoporosis, to study the change in the frequencies that make up the bone.

Another future path could entail the integration into a 2D or 3D auto-encoder to stitch together small volumes of bone into a larger one. This has been one of the major hurdles in the generation of realistic bone data, the size of the patches that can be generated. One such algorithm was implemented in [6] which was able to generate small volumes of bone. It is possible to generate bone samples with specific microstructural parameters. However, for larger volumes numerical instabilities make it impossible to generate realistic bone data to the desired specifications. An autoencoder with insight into a bone's isotropic properties at specific frequencies may be able to overcome the problem. It may be able to "stitch" together smaller volumes using the isotropic properties at the right scales to ensure proper boundaries.

Bibliography

[1] Nicolas Bonnet, Gerald Lemineur, Christine Chappard, Rachid Harba, and Claude-Laurent Benhamou. A new anisotropy index on trabecular bone radiographic images using the fast fourier transform. BMC medical imaging, 5:4, 06 2005. doi: 10.1186/1471-2342-5-4.

[2] Akbar Darabi, Florent Chandelier, and Gamal Baroud. Thickness analysis and reconstruction of trabecular bone and bone substitute microstructure based on fuzzy distance map using both ridge and thinning skeletonization. Electrical and Computer Engineering, Canadian Journal of, 34:57 – 62, 02 2009. doi: 10.1109/CJECE.2009.5291208.

[3] D.W. Dempster. The impact of bone turnover and bone-active agents on bone quality: Focus on the hip. Osteoporosis International, 13:349–352, 05 2002.

[4] Manoj Diwakar and Manoj Kumar. A review on ct image noise and its denoising. Biomedical Signal Processing and Control, 42:73–88, 2018. ISSN 1746-8094. doi: https://doi.org/10.1016/j.bspc.2018.01.010. URL https://www.sciencedirect.com/science/article/pii/S1746809418300107.

[5] Indranil Guha, Syed Ahmed Nadeem, Chenyu You, Xiaoliu Zhang, Steven Levy, Ge Wang, James Torner, and Punam Saha. Deep learning based high-resolution reconstruction of trabecular bone microstructures from low-resolution ct scans using gan-circle. volume 11317, page 29, 02 2020. doi: 10.1117/12.2549318.

[6] Emmanuel Iarussi, Felix Thomsen, and Claudio Delrieux. Generative Modelling of 3D In-Silico Spongiosa with Controllable Micro-structural Parameters, pages 785–794. International Conference on Medical Image Computing and Computer Assisted Intervention. 09 2020. ISBN 978-3-030-59724-5. doi: 10.1007/978-3-030-59725-2_76.

[7] Daniel Jiwoong Im, Sungjin Ahn, Roland Memisevic, and Yoshua Bengio. Denoising criterion for variational auto-encoding framework, 2015. URL https://arxiv.org/abs/1511.06406.

[8] Bruno Josso, David Burton, and Michael Lalor. Texture orientation and anisotropy calculation by fourier transform and principal component analysis. Mechanical Systems and Signal Processing, 19:1152–1161, 09 2005. doi: 10.1016/j.ymssp.2004.07.005.

[9] Jianfeng Kang, Enchun Dong, Shuangpeng Dong, Chen Zhang, and Ling Wang. Anisotropy characteristics of microstructures for bone substitutes and porous implants with application of additive manufacturing in orthopaedic. Materials Design, 191:108608, 02 2020. doi: 10.1016/j.matdes.2020.108608.

[10] Richard Ketcham and T Ryan. Quantification of anisotropy in trabecular bone. Journal of microscopy, 213:158–71, 03 2004. doi: 10.1111/j.1365-2818.2004.01277.x.

[11] William P. Shuman, Doug E. Green, Janet M. Busey, Orpheus Kolokythas, Lee M. Mitsumori, Kent M. Koprowicz, Jean-Baptiste Thibault, Jiang Hsieh, Adam M. Alessio, Eunice Choi, and Paul E. Kinahan. Model-based iterative reconstruction versus adaptive statistical iterative reconstruction and filtered back projection in liver 64-mdct: Focal lesion detection, lesion conspicuity, and image noise. American Journal of Roentgenology, 200(5):1071–1076, 2013. doi: 10.2214/AJR.12.8986. URL https://doi.org/10.2214/AJR.12.8986. PMID: 23617492.

[12] Felix Thomsen. Medical 3D image processing applied to computed tomography and magnetic resonance imaging. PhD dissertation, Universidad Nacional del Sur, 2017.

[13] Felix Thomsen, Claudio Delrieux, Juan Pisula, J.M. Fuertes, Manuel Lucena LÃşpez, Rodrigo GarcÃŋa, and Jan Borggrefe. Noise reduction using novel loss functions to compute tissue mineral density and trabecular bone volume fraction on low resolution qct. 11 2020.